Third International Conference on CFD in the Minerals and Process Industries
CSIRO, Melbourne, Australia
10-12 December 2003

HYDRODYNAMICS OF A PARTICLE IMPACT ON A WALL

Mark THOMPSON[1], Thomas LEWEKE[2], Alex CHEUNG[1] and Kerry HOURIGAN[1]

[1] Fluids Laboratory for Aeronautical and Industrial Research (FLAIR), Department of Mechanical Engineering, Monash University, Victoria 3800, AUSTRALIA

[2] Institut de Recherche sur les Phénomènes Hors Equilibre (IRPHE), CNRS / Université s Aix-Marseille, F-13884 Marseille, France

ABSTRACT

The problem of a particle impacting on a wall, a common phenomenon in particle laden flows in the minerals and process industries, is investigated computationally using a spectral element method with grid adjusting to the movement of the particle towards the wall. The assumed particle geometries studied are the generic two-dimensional and three-dimensional geometries of bluff body flows, the circular cylinder and the sphere. The principal case reported here is that of a particle impacting normal to the wall and sticking. The impacts are studied for moderate Reynolds numbers of the order 100 to 1200. A cylindrical body impacting on a wall is found to produce two vortices from its wake that convect away from the cylinder along the wall before stalling. In the case of a sphere, a pair of counter-rotating vortex rings is formed which strikes the wall. The dominant vortex ring of the pair consists of vorticity from the wake and persists and convects outwards away from the sphere, due to the induced motion from its image vortex. Vorticity fields and traces of passive particles originally resident on the wall are used to follow the interaction of the vortical structures. The evolution of the position and strength of the main vortex ring is quantified. For a Reynolds number greater than approximately 1000, the ring produced by an impacting sphere undergoes an instability in the azimuthal direction to produce a series of vortex loops with radial vorticity. Experimental visualisation using dye carried out in water is presented to validate the predictions.

NOMENCLATURE

D	diameter of particle
Re	$\equiv$ U D / ν, Reynolds number
t	$\equiv \tau$ U / D, normalised time
U	velocity of particle
τ	time
ν	kinematic viscosity

INTRODUCTION

Many processes in the minerals and process industries involve the transport and processing of particle laden fluids. Particle impacts on walls are a source of heat transfer augmentation as well as erosive wear and deposition (Joseph *et al.*, 2001). Surprisingly, very little visualisation of the fluid mechanics due to the impact of particles on surfaces has been undertaken. The recent article by Eames & Dalziel (2000) shows that when a rigid body collides with a surface, a layer of dust on the surface can be resuspended due to the effects of two different mechanisms. The first is a ballistic mechanism. The collision breaks cohesive bonds between the dust particles and, if the kinetic energy is sufficiently large, this can lead to the ballistic ejection of particles from the wall. For dust ejection by sand particles, experiments by Rice, Willetts & McEwan (1996), and Shao, Raupach & Findlater (1993) related the mass ejection rate to the collision rate and the energy loss per collision. The second mechanism leading to dust ejection is hydrodynamic; this is the focus of the current study. At Reynolds numbers in excess of approximately 100, the wake flow following the rigid body overtakes it on impact and the resultant ring vortex structure(s) can cause significant dust resuspension. More recently, Eames & Dalziel (2000) have examined the behaviour in more detail as the Reynolds number was varied between 300 and 3500. In that study, the analysis was primarily directed towards resuspension characteristics of different dust types and layer thicknesses rather than the fluid dynamics, which is of primary concern in this paper. Note that particle impacts with walls also have importance for other areas as well such as fouling and the enhancement of heat transfer due to the convection of fluid towards and away from the surface through the action of the wake structures.

In this paper the fluid dynamics associated with the impact is explored using both experimental and numerical methods. The cases of a cylindrical and a spherical body impacting normal to a wall and sticking are considered, with an emphasis on the dynamics of the vortex structures.

MODEL DESCRIPTION

Numerical Method

The spectral-element method (e.g., Karniadakis & Sherwin 1999) is employed to study the interaction numerically. An existing in-house axisymmetric spectral-element code, which has been validated extensively (e.g., Thompson, Leweke & Provansal 2001; Sheard, Thompson & Hourigan 2003), has been modified to treat the particle impact. The mesh modification is based on the ALE (Arbitrary Lagrangian-Eulerian) method described in Warburton & Karniadakis (1997). As the body moves towards the surface, the vertices of the mesh move with predetermined specified velocities so that the semi-circular boundary of the body (in the symmetric coordinate system) is maintained and the mesh does not become too distorted. The computational boundaries are placed sufficiently far from the body so that the blockage effect is negligible. A computational domain and mesh for the cylinder and the sphere are shown Figure 1. In the case of the sphere, this corresponds to the initial time before the

sphere is instantaneously accelerated downwards to a (non-dimensionalised) velocity of unity. For the simulations described in this paper, the initial distance from the wall was 25D, where D is the sphere diameter. This allows the wake to become almost fully-developed before the particle impact occurs. Although this distance is greater than in the experiments, the wake development and evolution will be found to be similar.

Visualisations from experiments performed after the numerical simulations indicated that it is difficult to maintain axisymmetry of the wake for initial distances beyond about 5-10D. Further numerical simulations are currently underway using the experimental distances, however, the predicted wake dynamics suggests that this change is unlikely to affect the main findings.

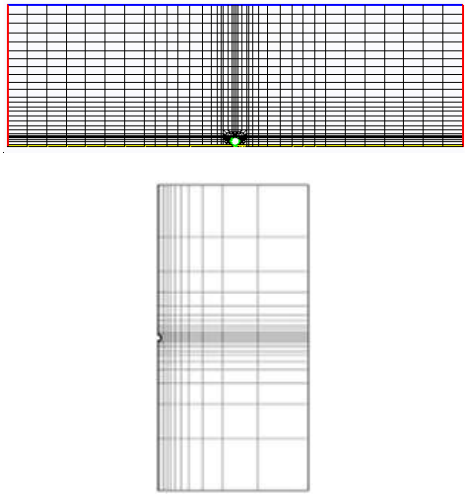

Figure 1: Mesh systems for the numerical calculation: top is cylinder mesh at time of impact and bottom is sphere mesh in the half (meridional) plane at initial time. The outer boundaries are at 25D from the sphere. Only macro-elements are shown.

The bodies are stopped at 0.005D from the wall to avoid mesh singularity problems. To show that this premature stopping did not have any significant effect on the results, simulations were repeated using a stopping distance of 0.05 diameters. The difference between the predictions in the two cases was negligible. Despite the significant final skewness of the mesh at that time, further time integration during the flow evolution stage is quite stable.

Experimental Techniques

The experiments were carried out in a 50x50x50 cm^3 glass tank filled with water. A metal ball 19.02 mm in diameter was attached to a fine twisted nylon thread. The thread passed over a pulley and was wound on a threaded reel driven by a computer-controlled stepper motor. This mechanism allowed the sphere to be lowered through the water at a specified speed, thereby allowing specification of the Reynolds number. Fluorescein dye and light from an Argon ion laser were used to visualise the wake vortical structures and the formation and advection of the vortex ring structures as the wake threaded over the sphere on impact. All of the experimental sphere impact studies were conducted with an initial distance from the wall of 5D.

RESULTS

Predicted Cylinder Collision with a Wall at Re = 100 and 200

The predicted two-dimensional results for two cases of different Reynolds number are presented here: Re = 100 and 200. The cylinder is considered because it is a generic two-dimensional bluff body that has been studied in detail in various other flows and represents one of the simplest two-dimensional bodies. At the low Reynolds numbers considered, it is expected that the assumption of two-dimensionality holds, particularly as the wake is not developed to unsteadiness before the collision with the wall occurs.

The results for the two cases are similar. The vorticity contour plots in figures 2 and 3 for Re = 100 and 200, respectively, show a series of snapshots beginning from when the cylinder initially strikes the wall. In these plots, the cylinder was initially moving vertically downwards. The horizontal black line on the bottom shows the position of the wall. The first plot in each figure is at the instant when the cylinder first makes ‘contact’ with the wall (Figures 2a and 3a). It shows vorticity forming on the wall as a result of fluid being pushed aside by the cylinder. In particular, the vorticity is generated by pressure gradients along the wall and diffused as the no-slip condition at the surface is satisfied. The sign of the vorticity is opposite to that of the primary vorticity of the wake for each half of the flow (i.e., above and below the centreline). After impact, the primary vortices continue to move forward due to self-induced motion and inertia. A secondary pair of vortices is formed on the surface of the cylinder as the primary pair (from the wake) overtakes the cylinder (Figures 2b and 3b).

The secondary vorticity of opposite sign formed at the cylinder surface appears in the flow again as a result of induced pressure gradients and diffusion as the no-slip condition is enforced. This vorticity from the cylinder surface then merges with vorticity generated at the wall to form vortex structures that wrap around the primary vortices that have convected away from the cylinder along the surface of the plate (Figures 2c and 3c). The approach of each primary vortex is cushioned by the secondary vorticity; the associated combined coherent structure slowly moves away laterally from the cylinder as time increases further. Towards the end of the simulation time, the structure moves only very slowly.

Figures 4 and 7 show the decay of the circulation of the primary vortex structure against time. The decrease of the strength of the circulation is almost linear with time between approximately 1 and 15 (Re = 100) and 1 and 12 (Re = 200) time units. At greater times, the rate of decay decreases; the decay rates are still approximately linear but the gradients are reduced. Thus, it appears that there are perhaps two different regimes. For smaller times, the generation of opposite-signed vorticity at the wall and cylinder surface and the associated cross-annihilation lead to initially rapid decay. for large times, new vorticity generation decreases and perhaps this results in a lower decay rate. Also for later times, the primary vortices begin to drift vertically away from the wall (as shown below); that is, there is a small “bounce” of the primary vortex by the positioning of the secondary vortices.

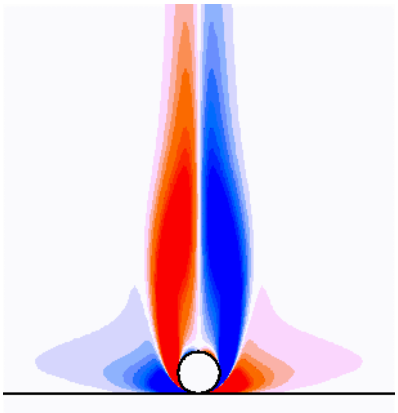

a) t = 0

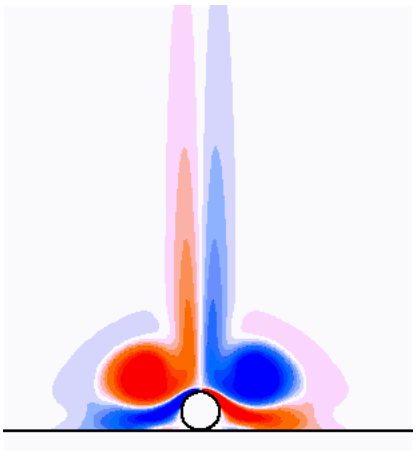

b) t = 10

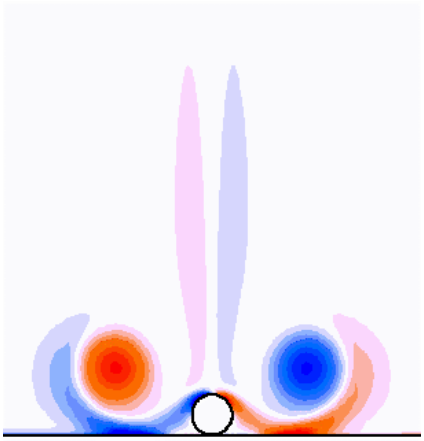

c) t = 25

Figure 2: Vorticity contour plots showing the evolution of the vorticity during impact and afterwards as the initially trailing wake overtakes the cylinder and interacts with the wall. The Reynolds number is 100.

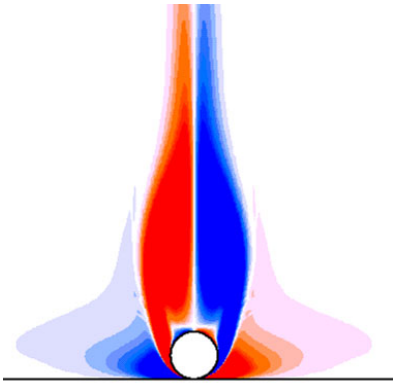

a) t = 0

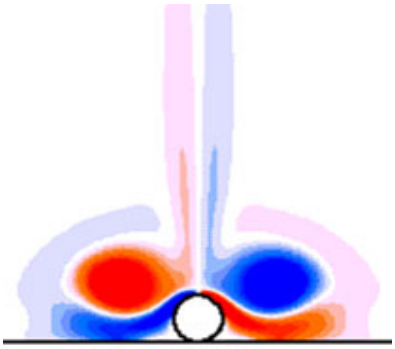

b) t = 10

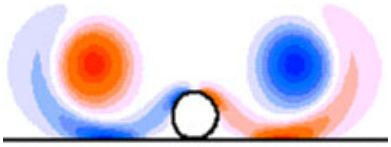

c) t = 25

Figure 3: As for Figure 2 but with Reynolds number 200 in this case.

This is consistent with the induced motion caused vorticity relative to the primary vortex. The mutual induction generates movement normal to the line joining the centres.

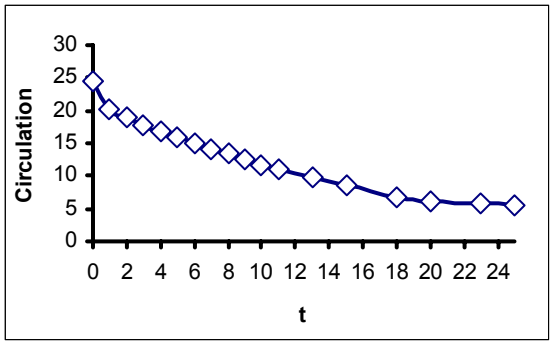

Figure 4: Variation of primary circulation with time for *Re*=100.

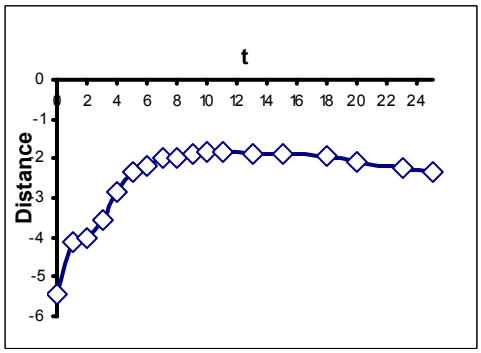

Figure 5: Vertical displacement (relative to D) of the primary circulation from the wall versus time for Re=100.

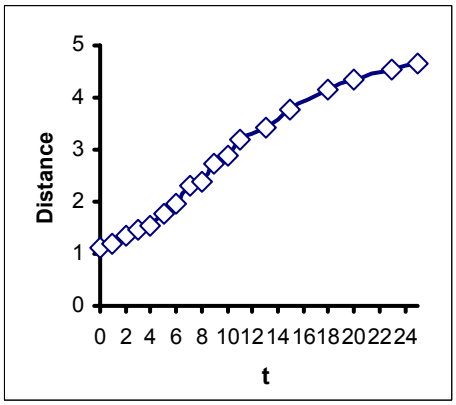

Figure 6: Horizontal displacement (relative to D) of the primary circulations against time for Re=100.

The vertical and horizontal displacements of the flow structures are shown in figures 5 and 6 (Re = 100) and 8 and 9 (Re = 200). The primary vortices (to the left and right of the centreline) move in towards the wall quickly as shown by the steep gradient in Figures 5 and 8. After approximately 5 time units, they start to slow due to induced vorticity and the presence of the boundary. After approximately 15 (Re = 100) and 12 (Re = 200) time units, the primary vortices begin to reverse direction. This is likely due to self-induced motion of the primary and secondary vorticity at this stage as discussed above.

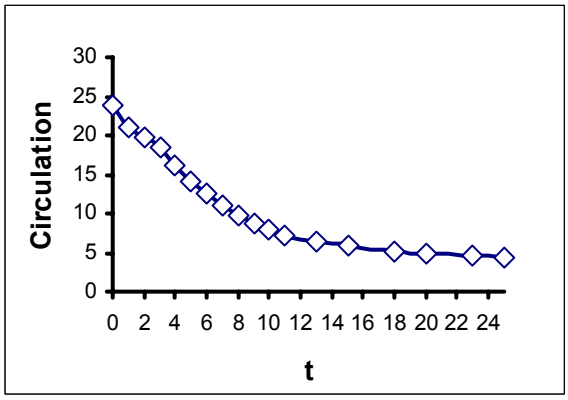

Figure 7: Variation of primary circulation with time for Re = 200.

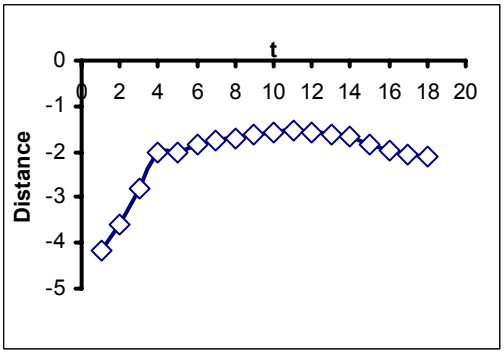

Figure 8: Vertical displacement (relative to D) of the primary circulation circulation from the wall versus time for Re = 200.

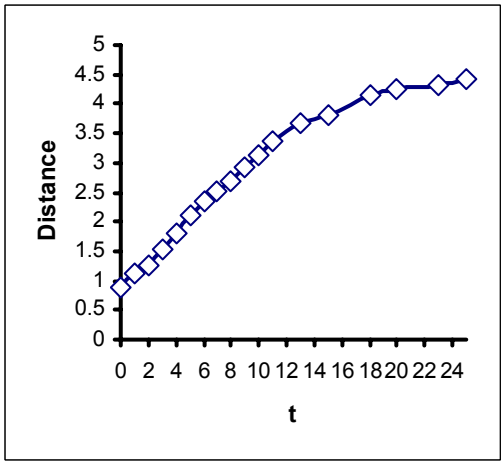

Figure 9: Horizontal displacement (relative to D) of the primary circulations versus time for Re = 200.

For the horizontal movement (Figures 6 and 9) though, there is much less of a demarcation between the behaviour at short and long times. There is a gradual decrease in the rate of change of position. It appears the asymptotic distance between the two primary vortices may be approximately 5-6 diameters, although this has

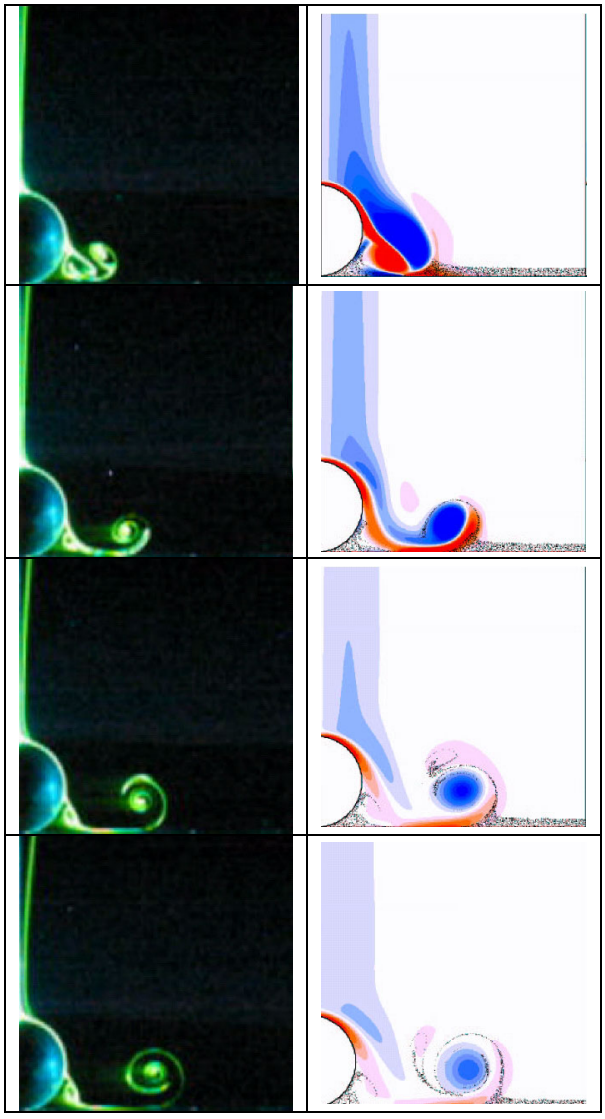

Figure 10: Non-dimensional times after impact of t = 2, 4, 8, 16, respectively. Experimental dye visualisations (left) and predicted vorticity and resuspended particle patterns (right) for sphere impact at Re = 500.

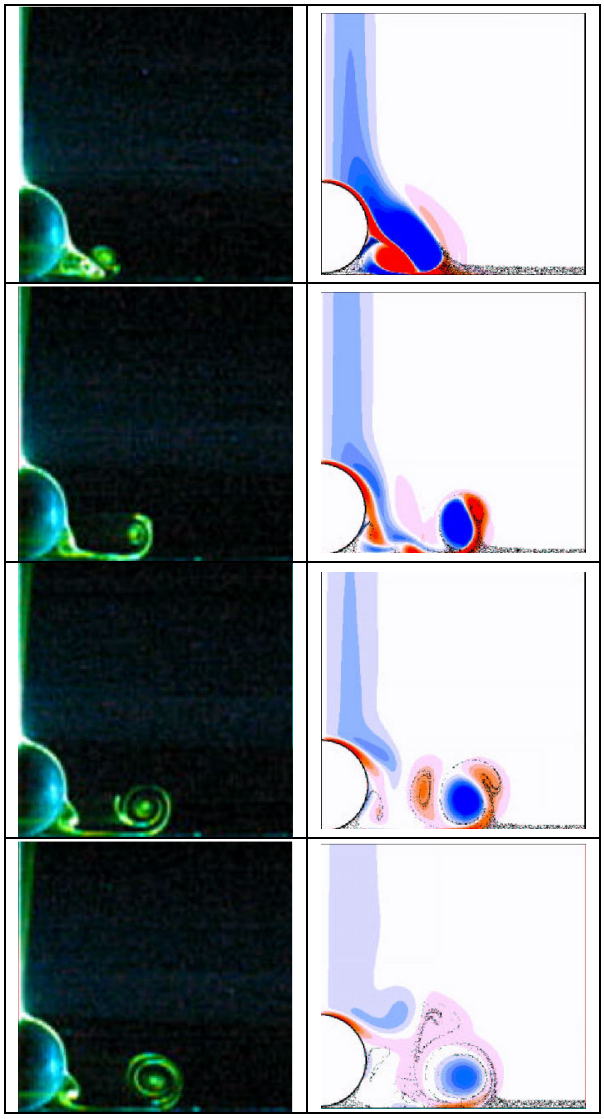

Figure 11: As for Fig. 10 but with Re = 800.

not been confirmed. For the case of Re = 200, the asymptotic distance appears to be slightly lower, probably closer to 5 diameters.

Sphere Collision with a Wall

Simulations were performed at Re = 100, 500, 800 and 1200. The evolution was followed for a non-dimensional time of at least 16 units after the collision. Visualisation of the numerical predictions was undertaken through the azimuthal vorticity distribution in the neighbourhood of the sphere. To investigate the effect on resuspension of small particles on the wall and to assist in the visualisation, massless tracer particles were introduced along the bounding wall at the time of impact. They were distributed randomly out to a thickness of 0.1D and their positions integrated in time. In this manner, we were able to visualise the effect of fine dust or dye at the surface.

For Re = 100 (not shown), the trailing wake threaded over the sphere on impact but there was little effect on the surface particles. No particles were actually ejected from the surface although there was a slight shifting of tracer particles due to the induced convective motion of the vortical ring structure. At t = 16, the vorticity originally from the wake had diffused and cross-annihilated substantially.

Figures 10 and 11 show the vortical flow patterns and tracer particle resuspension in the meridional (half) plane for Re = 500 and 800. The visualisations correspond to non-dimensional times of $t = \tau\, U/D = 2, 4, 8, 16$. (One time unit corresponds to the time taken for the sphere to move one diameter). The evolution of

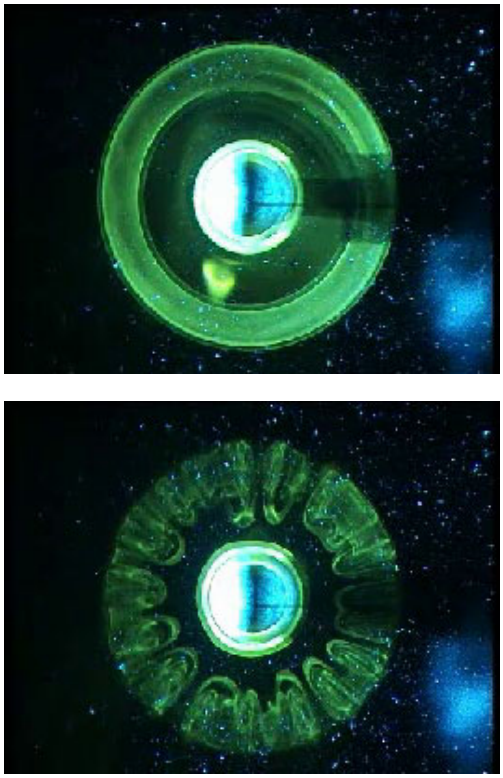

Figure 12: Bottom view of observed vortex ring for sphere impact at Re = 800 (upper) and Re = 1200 (lower).

the flow structures resulting from the impact are more interesting than for the lower (Re = 100) case described above. In both cases, a pair of counter-rotating vortex rings form as the anticlockwise vorticity from the wake passes over the top of the sphere and is paired with clockwise vorticity shed from the sphere surface. At approximately t = 2, the vortex pair reaches the surface and the particles are convected away from the region in which the pair strikes the surface. The diameter of the vortex ring was approximately 3.5D after t = 25. This is consistent with the experimental findings for the impact of a sphere (Eames and Dalziel, 2000).

The vorticity and particle distributions are similar at this time for the cases of Re = 500 and Re = 800. Over the next two time units, significant differences in the vorticity distributions develop within each case. The circulation from the wake is stronger than that generated at the surface of the sphere and hence the anticlockwise vorticity dominates.

The clockwise vorticity is wrapped around the anticlockwise vorticity at t = 4. There is still effectively a vortex (ring) pair at this time. For the higher Reynolds number case, the trailing clockwise vorticity breaks up into semi-discrete structures, whereas at the lower Reynolds number, the vorticity trails remain continuous. This is probably the result of a centrifugal instability which at the higher Reynolds number is not sufficiently damped to prevent the vorticity tails breaking up.

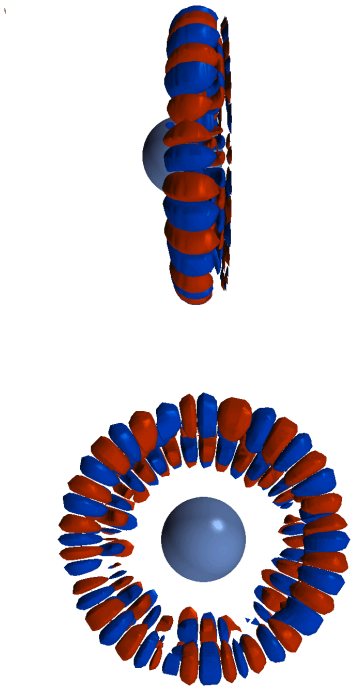

Figure 13: The predicted development of the radial component vorticity field (initially zero) for Re = 1200, after about 6 time units following impact; Side view (upper) and bottom view (lower).

At t =8, the effect is more pronounced with two distinct clockwise vortical satellites orbiting the still strong anticlockwise vortex ring. At a later time (not shown), three distinct clockwise vorticity satellites were clearly visible. In both cases, the region cleared out by the hydrodynamic interaction is similar but the particle distribution is considerably more complicated for the higher Reynolds number case. For Re = 800, the final snapshot at t=16 indicates that some of the anticlockwise vorticity from initial wake is being pulled around the established anticlockwise vortex ring, presumably due to the action of the clockwise rotating satellite vortices.

Three-Dimensional Instability of Vortex Ring

Experiments and three-dimensional numerical predictions were undertaken for the higher Reynolds numbers of 800 to 1200 to see if there was evidence of three-dimensional instabilities developing in the vortex rings formed from the sphere impact.

The experiments demonstrated that the first signs of instability waves around the ring appeared when the Reynolds number exceeded approximately 1000. For lower Reynolds numbers, the ring remained two dimensional, as shown for Re = 800 in Figure 12. When the Reynolds number was increased to 1200, the three-dimensional waves grew initially in the secondary vortex ring and then developed in the primary ring, as shown in the same figure, to form approximately 20 radial vortex loops.

The numerical predictions showed a similar result. At Re = 800, no three-dimensional instability developed. However, for Re = 1200, an instability was excited along the azimuth of the vortex ring and developed into loops of radial vorticity, as shown in Figure 13, in good agreement with the observation in Figure 12.

As the Reynolds number was increased further in the experiments, other wavelengths appeared in the vortex ring and the evolution became more complex.

The details of the experimental visualisations and the numerical predictions, e.g., time of vortex rings impact with the wall, final position of the ring vortex, and development and evolution of vortical structures, are seen to agree well. There is also general agreement with the predictions of Orlandi and Verzicco (1993) and Swearingen et al. (1995) for the case of a free vortex ring impacting on a solid boundary; in that case however, a longer azimuthal wavelength (n = 10) is found to be the most unstable mode.

CONCLUSIONS

A series of numerical predictions on the impact (and sticking) of both a circular cylinder and a sphere have been undertaken, with validating experiments. The spectral element method incorporating a deforming mesh based on the ALE (Arbitrary Lagrangian-Eulerian) method has successfully predicted the formation and evolution of a vortex pair (for the cylinder) or rings (for the sphere), validated by dye visualisation experiments. The spreading vortex ring, which appears to asymptote to a distance approximately 5 sphere diameters along the wall, is found to resuspend significant amounts of particles on the wall; it would be expected that the heat transfer rate properties would be also significantly modified by the influence of the ring.

As the Reynolds number is increased above approximately 1000, three-dimensionality appears in the spreading vortex ring. At Re = 1200, a single azimuthal wave is predicted and observed but more wavelengths appear as the Reynolds number is further increased.

Although the present studies are fundamental in nature and idealised, they do indicate that the hydrodynamic component of particle impacts on walls can be significant and may be an important factor in the transport properties and resuspension near walls in lightly loaded flows in the mineral and process industries.

ACKNOWLEDGEMENTS

This work has been supported by an ARC Linkage International grant and a CNRS international exchange grant. The computational studies have been supported by grants from the Victorian Partnership for Advanced Computing (VPAC) and the Australian Partnership for Advanced Computing (APAC).

REFERENCES

EAMES, I. and DALZIEL, S.B. 2000 Dust Resuspension by the Flow around an Impacting Sphere, *J. Fluid Mech*. 403, 305-328.

GONDRET, P., LANCE, M. & PETIT, L. 2002 Bouncing Motion of Spherical Particles in Fluids, *Phys. Fluids* 14, 2, 643-652.

JOSEPH, G.G., ZENIT, R., HUNT, M.L. & ROSENWINKEL, A.M. 2001 Particle-Wall Collisions in a Viscous Fluid, *J. Fluid Mech*. 433, 329-346.

KARNIADAKIS, G.Em. & SHERWIN, S.J. 1999 *Spectral/hp Element Methods for CFD* Oxford University Press.

ORLANDI, P. & VERZICCO, R. 1993 Vortex Rings Impinging on Walls: Axisymmetric and Three-dimensional Simulations, 256, 615-646.

RICE, M.A., WILLETTS, B.B. & McEWAN, I.K. 1996 Wind Erosion of Crusted Solid Sediments, Earth Surface Processes and Landforms, 21, 279-293.

SHAO, Y., RAUPACH, M.R. & FINDLATER, P.A. 1993 Effect of Saltation Bombardment on the Entrainment of Dust by the Wind, *J. Geophys*. R. 98, 12719-12726.

SHEARD, G., THOMPSON, M.C. and HOURIGAN, K. 2003 From Spheres to Circular Cylinders: The Stability and Flow Structures of Bluff Ring Wakes, *J. Fluid Mech*. 492, 147-180.

SWEARINGEN, J.D., CROUCH, J.D. & HANDLER, R.A. 1995 Dynamics and Stability of a Vortex Ring Impacting on a Solid Boundary, *J. Fluid Mech*. 297, 1-28.

THOMPSON, M.C., LEWEKE, Th. and PROVANSAL, M. 2001 Kinematics and Dynamics of Sphere Wake Transition, *J. Fluids Struct*. 15, 3/4, 575-585.

WARBURTON, T.C. & KARNIADAKIS, G.Em. 1997 Spectral Simulations of Flow past a Cylinder Close to a Free Surface, *ASME paper FEDSM97-3389*.